

Cluster contribution to the X-ray background as a cosmological probe

Doron Lemze^{1*}, Sharon Sadeh¹, & Yoel Rephaeli^{1,2}

¹*School of Physics and Astronomy, Tel Aviv University, Tel Aviv, 69978, Israel*

²*Center for Astrophysics and Space Sciences, University of California, San Diego*

29 August 2021

ABSTRACT

Extensive measurements of the X-ray background (XRB) yield a reasonably reliable characterisation of its basic properties. Having resolved most of the cosmic XRB into discrete sources, the levels and spectral shapes of its main components can be used to probe both the source populations and also alternative cosmological and large-scale structure models. Recent observations of clusters seem to provide evidence that clusters formed earlier and are more abundant than predicted in the standard Λ CDM model. This motivates interest in alternative models that predict enhanced power on cluster scales. We calculate predicted levels and spectra of the superposed emission from groups and clusters of galaxies in Λ CDM and in two viable alternative non-Gaussian (χ^2) and early dark energy models. The predicted levels of the contribution of clusters to the XRB in the non-Gaussian models exceed the measured level at low energies and levels of the residual XRB in the 2 – 8 keV band; these particular models are essentially ruled out. Our work demonstrates the diagnostic value of the integrated X-ray emission from clusters, by considering also its dependences on different metallicities, gas and temperature profiles, Galactic absorption, merger scenarios, and on a non-thermal pressure component. We also show that the XRB can be used for an upper limit for the concentration parameter value.

Key words: clusters: XRB – clusters: alternative cosmological models

1 INTRODUCTION

The origin of the cosmic X-ray background (CXRB) is of considerable interest due to possible ramifications on the properties of the various classes of sources that contribute to it, such as clusters and other extragalactic sources. By estimating their CXRB contributions and accounting for Galactic absorption we can compare with measurements of the observed X-ray background (XRB). Since the discovery of the XRB (Giacconi et al. 1962) significant effort has been devoted to spectrally mapping the emission at energies in the range $10^{-1} - 10^2$ keV. The radiation has a power-law form with a spectral index of $\Gamma = 1.4$ above 1 keV; the spectrum $E \cdot I(E)$, where $I(E)$ is the spectral intensity, peaks at $E \sim 30$ keV and decreases exponentially at higher energies. Substantial uncertainties in the measurement of $I(E)$ are due to cross-calibration uncertainties (e.g., De Luce & Molendi 2004) and spatial variations reflecting the large-scale structure (Gilli et al. 2003; Yang et al. 2003).

It has been determined that the XRB is mostly the superposed emissions from discrete extragalactic sources, other than at the lowest energies, $\lesssim 0.25$ keV, where its dominant contribution is thermal emission from the local bubble (LB) and the Galactic halo. Estimated fractional contributions of resolved sources to the XRB are 70–80% in the ROSAT 0.5 – 2 keV (Hasinger et al. 1998) and HEAO-1 A2 2 – 10 keV (Mushotsky et al. 2000) bands. Other estimates of the fractional contributions of resolved sources are 60–80% (Giacconi et al. 2001), 70% in the 2–8 keV band (Cowie et al. 2002). More recently, Worsley et al. (2005) determined XRB fractions of 85%, 80%, 60%, 50% for the 0.5–2, 2–10, 6–10, 8–10 keV bands, respectively. Higher fractions were deduced from deep Chandra fields (CDFs), $89.5_{+5.9}^{-5.7}\%$ and $86.9_{+6.6}^{-6.3}\%$ of the in the 0.5–2 and 2–8 keV bands, respectively (Bauer et al. 2004). These contributions include AGN, which dominate above 1 keV (Hasinger 2004, Brandt & Hasinger 2005 and references therein; Gilli, Comastri, & Hasinger 2007), star forming galaxies, and Galactic stars, but do not include emission from high-mass groups and clusters of galax-

* E-mail: doronl@wise.tau.ac.il

ies (which will be simply referred to as clusters); see also (Hickox & Markevitch 2006,2007).

A small contribution at very low energies may come from the warm hot intergalactic medium (WHIM). Most of the unresolved 1-2 keV emission can be accounted for by galaxies that are detected in deep HST observations, but are too faint to be detected as individual X-ray sources, as shown by a stacking analysis (Worsley et al. 2006). Analysis of the CDFs implies that the maximum contribution of clusters is estimated to be $\sim 17\%$ and $\sim 20\%$ in the 0.5-2 keV and 2-8 keV bands, respectively. Clusters are important probes of the primordial density fluctuation spectrum and the evolution of the large scale structure. Since conditions in clusters can be gauged by levels of X-ray emission, their estimated contribution to the CXRB can be used as a statistical diagnostic measure of the cluster population and its evolution.

The contribution of clusters to the XRB was estimated in several works (e.g., Rosati et al. 1998; Gilli, Risaliti, & Salvati 1999; Wu & Xue 2001) to be less than $\sim 10\%$ of the XRB spectral intensity at ~ 1 keV, and even lower at energies > 2 keV. The integrated spectral intensity of clusters can now be calculated more accurately from our improved knowledge of intracluster (IC) gas properties, the relevant scaling relations, as well as more precisely determined values of the global cosmological parameters. Moreover, X-ray line emission, which contributes significantly to the spectrum at low energies, particularly in high-mass groups, should be added to the thermal Bremsstrahlung emission (as has already been shown by Phillips, Ostriker, & Cen 2001).

Additional motivation for revisiting the issue of cluster contribution to the CXRB is provided by the possibility of using it to constrain alternative cosmological and LSS (Large scale structure) models, that have been proposed to remove apparent tension between the predictions of the standard model and recent observations of clusters. Possibly discrepant results include the following: (a) The detection of proto-spheroidal galaxies at $z \simeq 2$ with a substantially higher comoving density than what is predicted by most semi-analytic models of galaxy formation (Magliocchetti et al. 2007). Even more problematic is the detection of structures with high velocity dispersions at redshifts $z = 4.1$ (Miley et al. 2004) and $z = 2.1$ (Kurk et al. 2004). (b) The ‘excess’ CMB power at high multipoles ($l \approx 3000$) measured by the CBI (Readhead et al. 2004), ACBAR (Kuo et al. 2004), and BIMA (Dawson et al. 2006) arrays. The measured power levels seem to be too high to be comfortably consistent with the predicted CMB primary anisotropy, and are also outside the range of predicted anisotropy induced by the S-Z effect (Sadeh, Rephaeli, & Silk 2006, 2007). (c) High values of the concentration parameter, which were deduced for A1689 from two independent analyses: a joint lensing and X-ray analysis (Lemze et al. 2008a, hereafter L08a), and a dynamical analysis (Lemze et al. 2008b, hereafter L08b) of this cluster. In addition, high concentrations can explain the recently measured large Einstein radii in five high-mass clusters (Broadhurst & Barkana 2008), obtained from the analysis of high-quality ACS and Subaru lensing measurements and Chandra data. These values prove to be high even after relaxing the recent formation time assumption usually adopted in theoretical estimations, by considering the prob-

ability distribution function of halo formation times (Sadeh & Rephaeli 2008).

All the above apparently discrepant observational results can be naturally explained in the context of LSS models with primordial density fluctuation spectrum that had excess power on cluster scales, resulting in earlier formation and higher abundances of high-mass clusters than in the standard Λ CDM model. Several such viable models with the desired enhanced power on cluster scales are non-Gaussian χ^2 models (e.g., Koyama, Soda & Taruya 1999) and early dark energy models with time-varying coefficient of the quintessence equation of state (Doran et al. 2001; Caldwell et al. 2003). It has already been suggested by Mathis, Diego, & Silk (2004) that scale-dependent non-Gaussianity (at a level consistent with observational constraints from WMAP measurements) may be probed through its detectable manifestations on clusters. The predicted S-Z power spectra and cluster number counts were determined by Sadeh, Rephaeli, & Silk (2006, 2007).

Earlier formation, higher abundances, and more concentrated IC gas profiles will also be reflected in possibly discernible differences in their X-ray properties when compared with those predicted in the standard Λ CDM model. Therefore, in addition to the need to update and improve calculations of the contribution of clusters to the CXRB, further motivation for extending our previous work on alternative cosmological models is provided by the expectation that cluster X-ray properties could yield additional useful constraints on these models.

This paper is arranged as follows: In § 2 we describe the methodology adopted for the calculation of the spectral contribution of clusters and high mass groups in three distinct cosmological models. We present our results in § 3, where predicted XRB levels are made for alternative cosmological models, different levels of Galactic absorption, various gas profiles, cluster mergers, and in the case when the total gas pressure includes a non-thermal component. We conclude with a discussion in § 4.

2 METHODOLOGY

X-ray emission from clusters is calculated in Λ CDM, non-Gaussian (NG), and early dark energy (EDE) models. In the NG models the probability distribution function (PDF) of the primordial density fluctuation field has a χ_m^2 form. The largest deviation from Gaussianity occurs when there is one such field ($m = 1$). We consider the $m = 1$ and $m = 2$ cases. A full account of the the non-Gaussian and early dark energy models that we have used are provided in Sadeh, Rephaeli, & Silk (2006, 2007). Here we present a brief summary of the most important aspects which are of particular relevance to this work.

2.1 Λ CDM and Non-Gaussian Models

The number density of clusters as a function of mass and redshift is calculated using the Press-Schechter (Press & Schechter 1974, hereafter PS) mass function

$$\frac{dn(M)}{dM} = \frac{\bar{\rho}_m}{M} \frac{d\sigma}{dM} F(\nu), \quad (1)$$

where

$$F(\nu) = \begin{cases} N \sqrt{\frac{1}{2\pi}} e^{-\frac{\nu^2}{2}} \frac{\nu}{\sigma} \\ N \frac{(1+\sqrt{2/m\nu})^{m/2-1}}{(2/m)^{(m-1)/2} \Gamma(m/2)} e^{-m/2(1+\sqrt{m/2\nu})} \frac{\nu}{\sigma} \end{cases}. \quad (2)$$

The top and bottom expressions refer to the Gaussian and χ_m^2 models, respectively, and N is a normalization factor, introduced in order to arrange that all the matter in the universe will be incorporated into halos.

For the Gaussian, NG ($m=1$), and NG ($m=2$) models, $N = 2, 0.31, 0.37$, respectively. Additional quantities appearing in the PS mass function include $\nu \equiv \frac{\delta_c(z)}{\sigma(M)}$, which denotes the critical density for collapse in units of the mass variance. The latter quantity is defined as $\sigma^2(M) = \frac{1}{(2\pi)^3} \int d^3k \widetilde{W}_{TH}^2(kR) P(k)$, where $\widetilde{W}_{TH}(kR) = \frac{3}{(kR)^3} [\sin(kR) - kR \cos(kR)]$ is the Fourier transform of the Top-Hat window function, and the relation between M and R is $R = \left(\frac{3M}{4\pi\rho_{bg}}\right)^{1/3}$. The power spectrum is taken as $P(k) = A_p k^n T^2(k)$, with $n = 1$ and $n = -1.8$ for the Gaussian and NG models, respectively.

Adiabatic CDM and isocurvature transfer functions are used in the Gaussian and NG models:

$$T(k) = \begin{cases} \frac{\ln(1+2.34q)}{2.34q} [1 + 3.89q + (16.1q)^2 + (5.46q)^3 + (6.71q)^4]^{-0.25} \\ (5.6q)^2 [1 + \frac{(40q)^2}{1+215q+(16q)^2(1+0.5q)^{-1}} + (5.6q)^{8/5}]^{-5/4} \end{cases} \quad (3)$$

where $q \equiv k/(\Omega_m h^2) Mpc^{-1}$ (Bardeen et al. 1986), and A_p is the normalization set by σ_8 :

$$A_p = \frac{\sigma_8^2}{\frac{1}{2\pi^2} \int_0^\infty dk k^{n+2} T^2(k) \widetilde{W}_{TH}^2(8k)}. \quad (4)$$

The cosmological parameters were taken from the WMAP 3-year data, with $\Omega_\Lambda = 0.76$, $\Omega_m = 0.24$, $h = 0.73$, and $\sigma_8 = 0.74$ (Spergel et al. 2007). Due to the steep dependence of the cluster mass function on σ_8 , we have accounted for the higher value, ~ 0.82 , inferred from WMAP5 (Komatsu et al. 2008). This point is elaborated on in § 4. The gas profile is taken to be a β model, i.e. $n_{gas}(r) = n_{gas}(0)(1 + (\frac{r}{r_c})^2)^{-1.5\beta}$, where the central density is normalized such that the total gas mass constitutes a fraction 0.1 of the total cluster mass included within the virial radius, and r_c denotes the core radius. To allow for a temperature structure, the profile is taken to have a polytopic form, $T(r) = T(0)(1 + (\frac{r}{r_c})^2)^{-1.5\beta(\gamma-1)}$, where γ is the polytopic index, and the central temperature can be derived under the assumption of hydrostatic equilibrium (HE), that yields

$$T(r=0) = \frac{\mu m_p G}{3\beta\gamma k_B} \frac{M_{vir}}{r_{vir}} \left[1 + \left(\frac{r_{vir}}{r_c}\right)^2 \right]^{1.5\beta(\gamma-1)+1} \left(\frac{r_{vir}}{r_c}\right)^{-2}, \quad (5)$$

where G , m_p , μ and k_B are the gravitational constant, proton mass, mean molecular weight, and the Boltzmann constant, respectively.

We first consider isothermal gas, $\gamma = 1$, and take $C_{gas} \equiv \frac{r_{vir}}{r_c} = 10$, $\beta = \frac{2}{3}$. Note that C_{gas} is the virial radius in units of the gas core radius, essentially the analogous concentration parameter, where the virial radius is in units

of the NFW (Navarro, Frenk, & White 1997) scale radius. We consider (in § 3.3) a range of values of C_{gas} and γ in order to assess the dependence on these parameters. With the gas density and temperature profiles specified, we can calculate the spectral luminosity of a cluster with mass M and redshift z

$$L_{M,z}(E) = \int_0^{r_{vir}} \varepsilon_E dV, \quad (6)$$

where ε_E is the specific (spectral) emissivity in $erg \ sec^{-1} \ cm^{-3} \ keV^{-1}$. We compute the emissivity with the MEKAL plasma code and compare with results obtained when the emissivity includes only Bremsstrahlung continuum (Fig. 1). The calculation of the Gaunt factor was carried out using the analytic fitting formula of Itoh et al. (2000).

We consider all systems in the mass range $1.1 \cdot 10^{13} - 7.3 \cdot 10^{15} h_{0.7}^{-1} M_\odot$, which roughly includes all halos larger than a cD galaxy. Increasing the upper halo mass limit does not affect the results, since the PS formalism predicts an extremely low abundance of such massive halos. Indeed, the most massive currently known cluster, A370, has a mass $(2.93_{-0.32}^{+0.36} \cdot 10^{15} h_{0.7}^{-1} M_\odot)$, Broadhurst et al. 2008) which is less than half the assumed upper end of this range. The specific flux from all clusters in this mass range is

$$F(E) = \int_0^{z_{max}} dz \int_{M_{min}}^{M_{max}} L_{M,z}(E) \frac{dn(M,z)}{dM dz} \frac{1}{4\pi D_L^2(z)} dM, \quad (7)$$

where D_L is the luminosity distance; in our calculations we take $z_{max} = 3$.

2.2 EDE Model

The evolutionary history in the EDE model is different from that in the Λ CDM universe, for which we used the Gaussian and NG models. The vacuum (Quintessence) energy density, $\rho_Q(z)$, is redshift dependent,

$$\rho_Q = \rho_{Q_0} (1+z)^{3[1+\overline{\omega}(z)]}, \quad (8)$$

where $\overline{\omega}(z)$ is the equation of state coefficient (-1 for a cosmological constant). In our calculations we adopt the parametrisation of Wetterich (2004):

$$\overline{\omega}(z) = \frac{\omega_0}{1 + u \log(1+z)}, \quad (9)$$

and $u \equiv \frac{-3\omega_0}{\log \frac{1-\Omega_e}{\Omega_c} + \log \frac{1-\Omega_m}{\Omega_m}}$, where Ω_e is the early quintessence density and ω_0 is $\omega(z=0)$. The specific EDE model assumed here is that investigated by Bartelmann, Doran, & Wetterich (2006; hereafter BDW), for which $\Omega_e = 8 \cdot 10^{-4}$ and $\omega_0 = -0.99$.

Several cosmological quantities which are affected by the presence of early dark energy require re-evaluation. These include the (comoving) radial and angular diameter distances, linear growth factor, the critical density for spherical collapse, and the overdensity at virialization, all of which are explicitly calculated by Sadeh, Rephaeli, & Silk (2007).

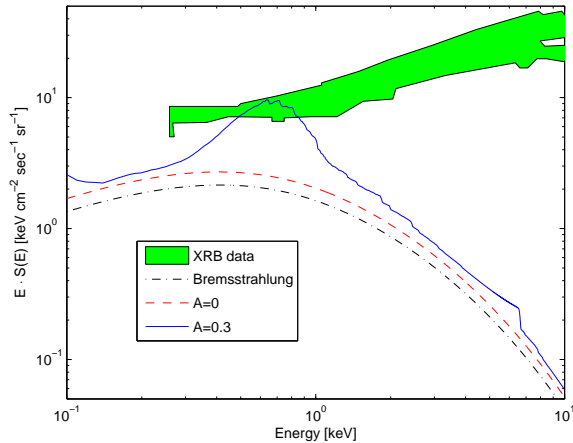


Figure 1. The integrated contribution of clusters and high mass groups with masses $(1.1 \cdot 10^{13} - 7.3 \cdot 10^{15}) h_{0.7}^{-1} M_{\odot}$ to the XRB intensity as a function of energy is shown together with the XRB data. Emission processes include free-free (black dash-dotted curve), optically thin hot plasma with zero metal abundance, $A=0$ (red dashed curve), and optically thin hot plasma with $A=0.3$ (blue solid curve).

3 RESULTS

3.1 Cluster contribution to the CXRB in Λ CDM

As noted, we have used the MEKAL code to calculate gas emissivity. Inclusion of only Bremsstrahlung continuum emission appreciably underestimates radiation from hot plasmas, especially at the relatively low temperatures of the more abundant groups and poor clusters, for which line emission at low energies and continuum free-bound emission processes should also be included. In Fig. 1 we show the superposed spectrum of clusters in the mass range $1.1 \cdot 10^{13} h_{0.7}^{-1} M_{\odot} - 7.3 \cdot 10^{15} h_{0.7}^{-1} M_{\odot}$ when including only free-free emissivity (dash-dotted line), optically thin hot plasma with zero metal abundances, $A=0$ (dashed line), and optically thin hot plasma with $A=0.3$ (solid line). The XRB measurements (with uncertainties), shown here by the green region, are based on the compilation of Gilli et al. (2007), who combined measurements from HEAO-1 (Gruber 1992; Gruber et al. 1999), ASCA GIS (Kushino et al. 2002), ROSAT PSPC (Georgantopoulos et al. 1996), two different sets of XMM measurements (Lumb et al. 2002; De Luca & Molendi 2004), ASCA SIS (Gendreau et al. 1995), BeppoSAX (Vecchi et al. 1999), RXTE (Revnivtsev et al. 2003), and shadowing experiments (Warwick & Roberts 1998). These measurements differ slightly in their minimum Galactic latitude. The effect of different minimum Galactic latitudes on the spectrum is investigated in § 3.2. As can be inferred from Fig. 1, the level of the Bremsstrahlung emission alone is quite low in comparison with the XRB measurements. Its contribution peaks at ~ 0.4 keV, where it constitutes $\sim 20\%$ of the CXRB. Inclusion of the full continuum (Bremsstrahlung and free-bound) with $A=0$ enhances the cluster emissivity by ~ 1.25 across the entire $0.1 - 10$ keV energy band. With the higher abundance of $A=0.3$, the emissivity is much higher, especially in the $0.4 - 1$ keV energy band.

Clearly, high mass groups and clusters contribute to

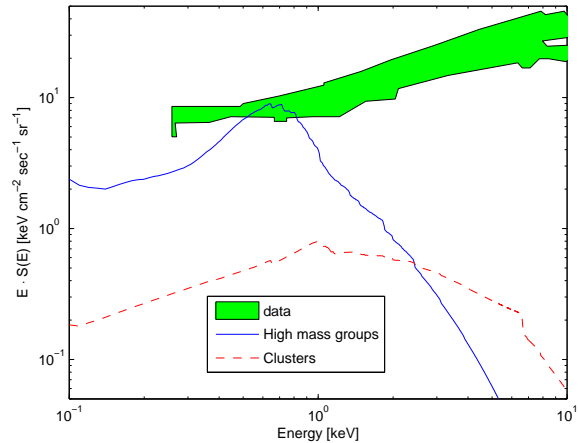


Figure 2. The relative XRB spectral intensity contributed by high-mass groups and clusters, defined by the respective mass ranges of $1.1 \cdot 10^{13} h_{0.7}^{-1} M_{\odot} - 10^{14} h_{0.7}^{-1} M_{\odot}$ and $10^{14} h_{0.7}^{-1} M_{\odot} - 7.3 \cdot 10^{15} h_{0.7}^{-1} M_{\odot}$.

the CXRB in different energy bands. Clusters contribute at higher energies due to their higher masses. We illustrate in Fig. 2 the contribution of the two populations, where we took the mass range of the high mass groups and clusters to be $1.1 \cdot 10^{13} h_{0.7}^{-1} M_{\odot} - 10^{14} h_{0.7}^{-1} M_{\odot}$ and $10^{14} h_{0.7}^{-1} M_{\odot} - 7.3 \cdot 10^{15} h_{0.7}^{-1} M_{\odot}$, respectively. The former population dominates the emission below ~ 2.5 keV, whereas the latter contributes mostly at higher energies. Clearly, the superposed emission of the lower mass systems can be used to constrain models that predict large spectral bumps, whereas the higher mass clusters can be used to constrain models in which fractional contribution of clusters is higher than the low residual level, namely upon subtraction of the dominant AGN contribution.

We have explored the dependence of the predicted intensity on the various LSS quantities and IC gas model. Here we consider the impact of using approximate fitting formulae for the linear growth factor, critical density for spherical collapse, and overdensity at virialization. To do so we numerically solved the relevant equations describing these quantities (see, e.g., Sadeh, Rephaeli, & Silk 2007) and used these exact solutions instead of the respective approximate fitting formulae. We find that at low energies the two sets of calculations yield essentially the same results. However, with increasing energy the exact calculation yields a level of intensity which is lower by as much as $\sim 17\%$ at 10 keV, as can be seen in Fig. 3.

In the following subsections we assess the impact of IC gas modeling uncertainties, merger histories of clusters, and dependence of the predicted CXRB intensity on Galactic absorption.

3.2 Galactic absorption

To account for photoelectric absorption in the Galaxy, we combined our calculated CXRB intensity with the XSPEC WABS model. We then computed the average column density in the following way: 10^4 lines of sight (los) were picked at random with a uniform probability distribution on a

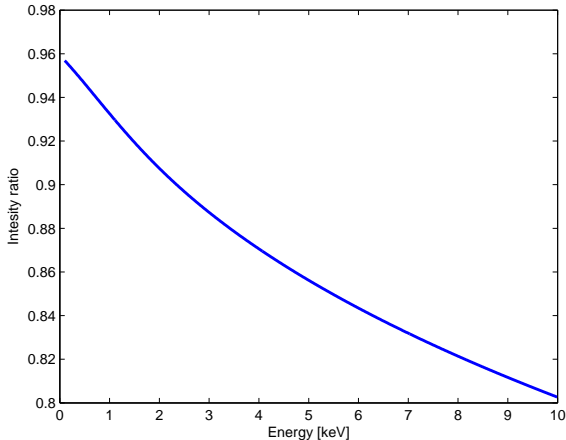


Figure 3. The spectral intensity calculated using analytical fits for the linear growth factor, critical density for spherical collapse, and overdensity at virialization, compared with the corresponding spectral intensity calculated using the exact numerical solutions to the differential equations for these quantities. (This comparison was made for the case $A = 0$.)

sphere. This number proved to be sufficient in order to produce statistically meaningful results by virtue of the fact that with 10^3 los the average column density changed negligibly and its error was still small. Note that the number of los has an upper limit of 41259 since the resolution of the column density is $\sim 1^\circ$.

For each los we obtained the column density using the *nh* tool (Dickey & Lockman 1990). This procedure was repeated 10 times, yielding the average column density and its standard deviation, which was taken to be the error. In this way we calculated the average column density of the Galaxy in all directions. In order to take into account the fact that XRB observations are performed at different Galactic latitudes, we calculated the average Galactic absorption at stripes of Galactic latitude $b > 10^\circ$ and $b > 30^\circ$, namely excluding the disk region, and the combined regions of the disk and the bulge, respectively. In addition, many X-ray observations point at regions on the sky where the column density is significantly lower, the goal of which is the detection of the soft X-ray background (which is absorbed in regions of high column densities). Such a region is the Lockman Hole, associated with a minimum hydrogen column density $N_H = (4.5 \pm 0.5) \cdot 10^{19} \text{ cm}^{-2}$ (Lockman et al. 1986).

Results for the average column density at different regions marked by the lower limit of the Galactic latitude are summarized in table 1. The contribution of clusters to the XRB with $A = 0.3$, taking into account the effect of Galactic absorption, but excluding the effect of mergers, is illustrated in Fig. 4.

3.3 IC Gas Density and Temperature Profiles

The density profile of IC gas is usually represented by a β model, which fits well X-ray and SZ measurements (though occasionally a double β model provides a better fit). However, the assumption of isothermality is known to be unreal-

Table 1. The average column density at latitudes higher than b . The Lockman hole is situated at $\alpha = 10^h 45^m$, $\delta = 57^\circ 20'$ (Lockman et al. 1986)

b [$^\circ$]	$\langle N_H(> b) \rangle$ [10^{20} cm^{-2}]
0	13.9 ± 0.3
10	6.05 ± 0.06
30	3.54 ± 0.04
Lockman hole	0.45 ± 0.05

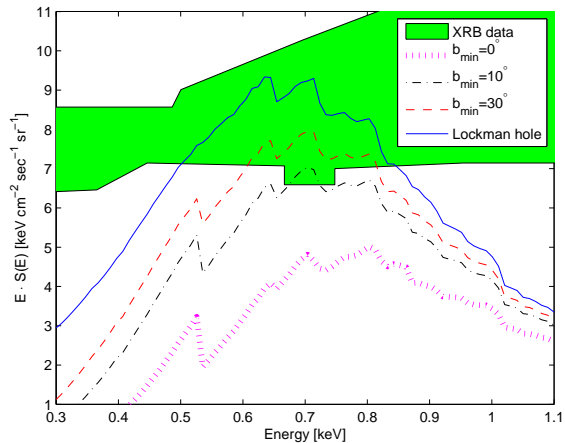


Figure 4. The impact of Galactic absorption on the integrated contribution of clusters and high mass groups to the XRB spectral intensity, for Galactic latitudes $b > 0^\circ$ (purple striped curve), $b > 10^\circ$ (black dash-dotted curve), $b > 30^\circ$ (red dashed curve), and the Lockman hole (blue solid curve)

istic, especially in the outer regions of clusters. A polytropic equation of state provides a more realistic temperature profile, since at $r \gg r_c$, $n(r) \propto r^{-3\beta}$ and $T(r) \propto r^{-3\beta(\gamma-1)}$.

We can use insight on the profile of the gas entropy parameter, $K \equiv T n^{-2/3}$, to select the relevant range of γ values. In the outer regions of clusters, $r \gtrsim 0.1 R_{\text{vir}}$, beyond the cool core, the entropy is entirely due to gravitational processes, and its profile is expected to be a featureless power law approaching $K \propto r^{1.1}$ (Tozzi & Norman 2001; Voit, Kay, & Bryan 2005). However, a recent model-independent analysis of X-ray and lensing measurements of A1689 yielded 0.82 ± 0.02 for the power-law index of the profile (L08a). For isothermal gas, $\beta = 2/3$ implies $K \propto r^{4/3}$. This value of the index is higher than the two aforementioned values of 1.1 and 0.82. Thus, in addition to not being realistic at large radii, the isothermal case is also inconsistent with the entropy profile when $\beta = 2/3$ is adopted. In order for the entropy profile to have an index of 0.82, γ has to be $\simeq 1.25$, which is in good agreement with both ASCA measurements of 30 nearby clusters (Markevitch et al. 1998) and numerical simulations (Loken et al. 2002).

In fig. 5 we explore the cluster contribution to the CXRB for different values of C_{gas} and γ . For $C_{\text{gas}} = 10$ and $\gamma = 1.25$ the X-ray intensity is higher at $E > 1$ keV as compared with its value for $\gamma = 1$, reflecting the higher central temperature. Although the temperature at $r \gtrsim r_{\text{vir}}$ is lower than in the $\gamma = 1$ case, the radial integration (to r_{vir})

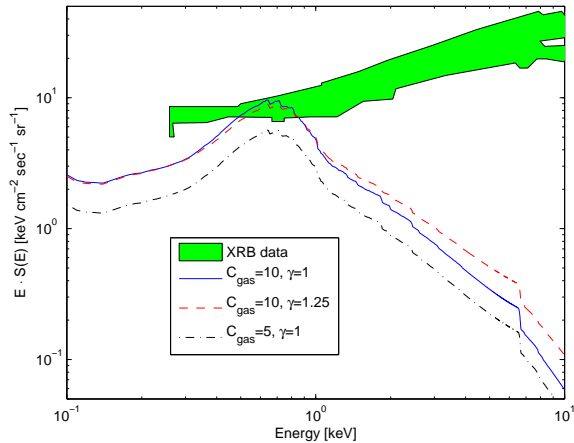


Figure 5. Dependence of the cluster CXRB contribution on different values of C_{gas} and γ .

only results in a boost of the intensity level at high energies. For $C_{gas} = 5$, there is no significant difference between the $\gamma = 1$ and $\gamma = 1.25$ cases, a result of which can be explained taking into account the fact that the change in the central temperature (which depends on C_{gas}) is lower, and that the core radius of the gas is bigger so that the range of difference between the core and the virial radii is smaller.

3.4 Impact of cluster mergers

The formation of structure in CDM models is hierarchical; clusters evolve through mergers of subclumps. During these merger events the temperature and luminosity of IC gas are temporarily boosted up with respect to the corresponding equilibrium values, in a manner that has been characterized by hydrodynamical simulations. Neglecting this boost may lead to an underestimation of the cluster contribution to the CXRB. Randall, Sarazin, & Ricker (2002, hereafter RSR02) employed a semianalytic model to estimate the effect of merger boosts on the X-ray luminosity function (XLF) and temperature function (TF). A quantification of the luminosity and temperature spikes in individual mergers was made based on N-body/hydrodynamical simulations, whereas the statistics of the merger history were determined from Extended PS (EPS) merger trees. RSR02 used these merger-booster TFs and XLFs to infer σ_8 and Ω_m by converting them to PS mass functions and comparing with local ($z = 0$) and distant (either $z = 0.5$ or $z = 1$) cluster samples. For the Λ CDM model an increment of 20% in σ_8 was deduced by fitting to both the TF and XLF. On the other hand, results for Ω_m were inconclusive; fitting to the TF and XLF exhibited a decrement and an increment, respectively. In fact, the results obtained from the XLF fit were less reliable, as indicated by the fact that Ω_m inferred from the non-booster functions was lower by 60% than the actual value used to construct the merger trees. The reason for the lower degree of reliability associated with the fit to the XLF is due to the fact that the range of X-ray luminosities is broader than that of X-ray temperatures; put otherwise, the X-ray luminosity-temperature scaling is steeper than a linear relation. As a

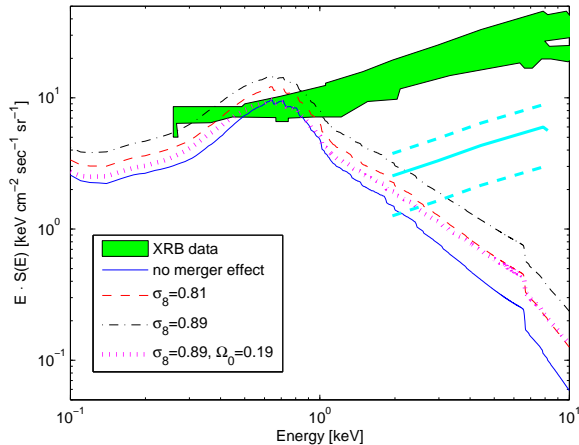


Figure 6. The cluster contribution to the CXRB including the effect of mergers. Plotted are the XRB data (green area), the cluster contribution without the effect of mergers (blue solid curve), and the corresponding contributions when their effect was modelled by selecting values of σ_8 higher by 10% and 20% (red dashed and black dot-dashed curves, respectively), and by increasing σ_8 by 20% but lowering Ω_m by 20% (purple striped curve). Also shown is the currently estimated upper limit on the residual (i.e., after accounting for emission from AGN) 2-8 keV emission and its 1- σ range (cyan solid and dashed lines, respectively).

result, the overall effect of luminosity boosts on the XLF is not as strong as the effect of temperature boosts on the TF.

The fitted σ_8 to the boosted TFs was higher by 20% than the value used to construct the trees, whereas with the non-booster TFs it was higher by only 10% (a difference which is due to the approximation used to determine the cluster formation redshift). In Fig. 6 we compare our calculated cluster contribution to the CXRB including the effect of mergers with the data. The impact of mergers was modelled in three different ways by selecting values of σ_8 higher by 10% ($\sigma_8 = 0.81$) and 20% ($\sigma_8 = 0.89$), and by adopting a combination of σ_8 higher by 20% ($\sigma_8 = 0.89$) and of Ω_m lower by 20% ($\Omega_m = 0.19$). As is clear from the figure, the third choice, i.e. the one combining a higher σ_8 and a lower Ω_m , would seem more likely, simply by virtue of its consistency with the data. In fact, this scenario was also preferred by RSR02, who noted that the effect of merger boosts on σ_8 and Ω_m depends somewhat on the detailed method used to determine the TFs and XLFs, and the criteria used to fit them. It should be noted that this holds for $C_{gas} = 10$; for $C_{gas} = 5$, none of the models exceed the observed intensity range. However, this is no longer the case if σ_8 is higher, as is alluded to in § 4. In addition, in the the 2 – 8 keV energy band high values of σ_8 boost the cluster CXRB contribution above the 1- σ upper limit of the residual XRB, which was calculated by multiplying the measured XRB upper bound (in the 2 – 8 keV band) by the residual fraction determined by Bauer et al. (2004).

Results for merger boosts that emerge from various works differ in several respects. Bullock et al. (2001) found in their simulations a value of λ_{med} , the spin parameter (Peebles 1971), lower than 0.05, the value used in RSR02. This would slightly increase the effect of merger boosts. On the other hand, preheating and non-gravitational effects may

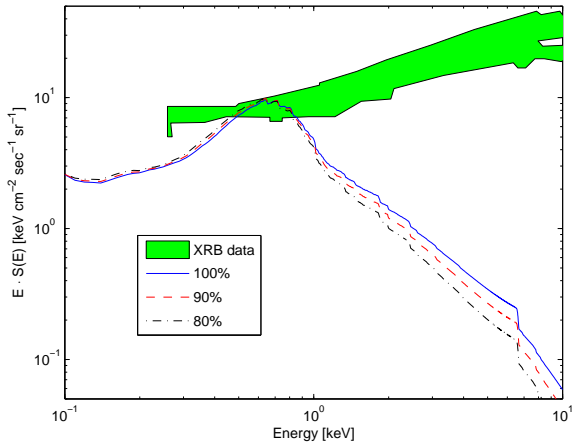


Figure 7. The cluster CXRB contribution for a purely thermal, and for the case when the thermal pressure is only 90 %, or 80% (blue solid, red dashed, black dot-dashes curves, respectively).

somewhat reduce the effect of merger boosts since the fractional increase in the X-ray luminosity and temperature would be smaller if non-gravitational heating is considered. This effect would dominate in low-mass clusters (Ponman et al. 1996).

3.5 Non-thermal pressure

The hydrostatic equation (HE) for an ideal gas can be integrated from a given radius r (assuming spherical symmetry) out to some limiting radius

$$[\rho_{gas}(r)T(r)] \Big|_r^\infty = C \int_r^\infty \frac{GM(\leq r')\mu m_p \rho_{gas}(r') dr'}{k_B r'^2}, \quad (10)$$

where ρ_{gas} and T are the gas mass density and temperature, respectively, $M(\leq r)$ is the total mass within radius r . If the only contribution to the pressure - which balances gravity - is the thermal gas, $C = 1$ (e.g., Binney & Tremaine 1987).

In our work so far we have assumed that clusters are in hydrostatic equilibrium, and that gas pressure is strictly thermal. However, this may not necessarily be the case, at least in some clusters. Accordingly, the impact of having a second pressure component was assessed heuristically (ignoring other possible ramifications of the source of the additional pressure), simply by gauging the lower IC gas contribution by taking $C = 0.9$ and $C = 0.8$ (assuming, rather realistically, that a non-thermal - such as turbulent and energetic particle - component does not exceed 20% of the total pressure). We can see from Fig. 7 that as C decreases the cluster contribution is lowered at energies > 1 keV, with practically no change at lower energies.

3.6 Seth & Tormen mass function

The PS mass function, which is derived under the naive assumption of spherical collapse, underpredicts the abundance of higher mass clusters, and overpredicts the abundance of lower mass systems, with respect to those observed in N-body simulations. Such simulations manifest a clear non-spherical collapse behaviour. Sheth & Tormen (1999,

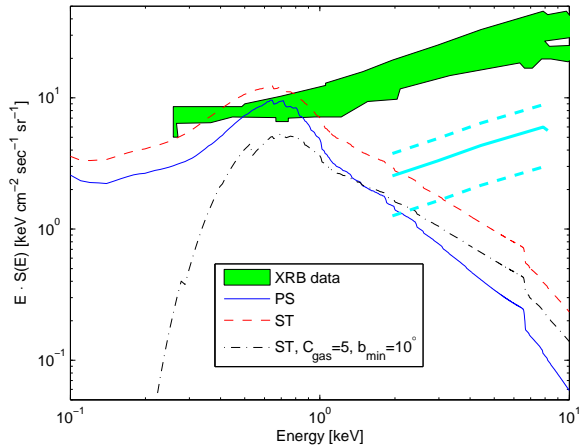


Figure 8. The cluster CXRB contribution calculated with the PS (solid line), ST (dashed line) mass functions; also shown is the result for ST mass function with $C_{gas} = 5$ and Galactic absorption with $b_{min} = 10^\circ$ (dash-dotted line). Also shown is the currently estimated upper limit on the residual (i.e., after accounting for emission from AGN) 2-8 keV emission and its 1- σ range (cyan solid and dashed lines, respectively).

hereafter ST; see also Maggiore & Riotto 2009) developed a modified mass function, which provides a better agreement with results of simulations (Sheth, Mo, & Tormen 2001):

$$F(\nu) = A \sqrt{\frac{2a}{\pi}} \left[1 + \left(\frac{\nu^2}{a} \right)^p \right] e^{-\frac{a\nu^2}{2}} \frac{\nu}{\sigma}, \quad (11)$$

where $A = 0.3222$, $a = 0.707$, and $p = 0.3$. The PS mass function is reproduced when $A = 0.5$, $a = 1$, and $p = 0$. In Fig. 8 we plot the CXRB spectrum in the mass range $1.1 \cdot 10^{13} h_{0.7}^{-1} M_\odot - 7.3 \cdot 10^{15} h_{0.7}^{-1} M_\odot$, using the PS (solid line) and ST (dashed line) mass functions, and the ST mass function with $C_{gas} = 5$ and Galactic absorption with $b_{min} = 10^\circ$ (dash-dotted line).

Since the ST mass function generates a higher population of high-mass halos with respect to the PS mass function in almost the entire considered mass range, it gives rise to a significant increase of the predicted spectrum. If we neglect Galactic absorption, the computed levels exceed the measured XRB range; if Galactic absorption is included, the power spectrum peaks at approximately the same level as the unabsorbed spectrum generated with the PS mass function. Since not all of the XRB in the $0.4 \lesssim E \lesssim 1$ keV energy range is due to clusters, their partial contribution actually puts a very strong constraint on the value of C_{gas} : As is clear from the figure, the ST mass function yields intensity levels which are roughly half of the observational upper limit, if Galactic absorption with $b_{min} = 10^\circ$ and $C_{gas} = 5$ are adopted. Note that the residual emission in the 2 – 8 keV band yields an upper limit of ~ 10 on C_{gas} .

3.7 Alternative cosmological models

As discussed in the § 1, there is considerable interest in viable alternative cosmological models that predict enhanced power on the scale of clusters, and their earlier formation than in Λ CDM. In this section we determine the CXRB

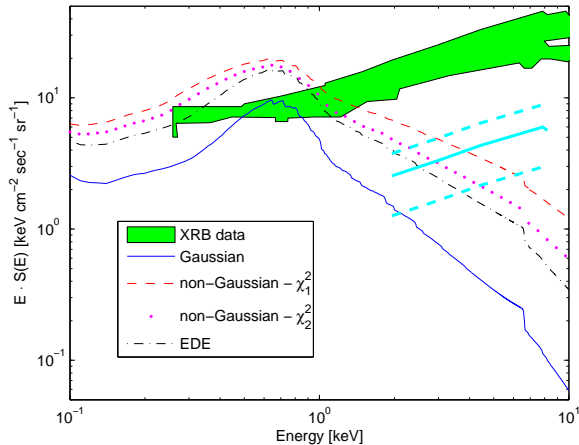


Figure 9. X-ray spectral intensity curves produced by a cluster population derived from a PS mass function with a Gaussian (solid line), χ_1^2 (dashed line), and χ_2^2 (dotted line) PDFs, and an EDE model (dot-dashed line). Also shown is the currently estimated upper limit on the residual (i.e., after accounting for emission from AGN) 2-8 keV emission and its $1-\sigma$ range (cyan solid and dashed lines, respectively).

cluster contribution in the NG and EDE models specified above. In Fig. 9 we compare the X-ray intensity spectra produced by a cluster population derived from a PS mass function with a Gaussian (solid line), χ_1^2 (dashed line), and χ_2^2 (dotted line) PDFs, and an EDE model (dot-dashed line). As is clear from Fig. 9, the predicted intensity levels in the NG models for both $m=1$ and $m=2$ are much higher than the observed range below ~ 1 keV. Clusters overproduce the XRB at a level which is well beyond the range of modeling uncertainties. The predicted level of contribution is in fact excessive also in the $0.5-2$ keV band, where clusters are presumed to contribute at most 10-20% of the measured XRB intensity. In the $2-8$ keV energy band the predicted intensity levels in these models are higher than the $1-\sigma$ upper limit of the residual XRB. This interesting result strengthens the conclusion of Sadeh, Rephaeli & Silk (2007) who showed that the level of CMB anisotropy induced by the S-Z effect is significantly higher than the current upper limits set by the BIMA experiment. Based on these excess intensity and power levels, these particular NG models seem to be ruled out.

The degree at which predictions of the EDE model may be reconciled with the observational constraints depends on the normalization of the matter power spectrum. With the same σ_8 as derived from WMAP, the intensity bump exceeds the XRB data, similar as in the non-Gaussian models. However, when we determine the value of σ_8 by requiring that the cumulative halo number at $z=0$ in this model matches the corresponding value in the Λ CDM we obtain essentially the same spectrum. The predictions for the surface brightness distribution as a function of mass and redshift are shown in Fig. 10 for the three models.

The level of tension between predictions of the EDE model and the CXRB measurements depends very much on the value of σ_8 . Normalizing σ_8 such that the cumulative halo number at $z=0$ in this model is roughly equal

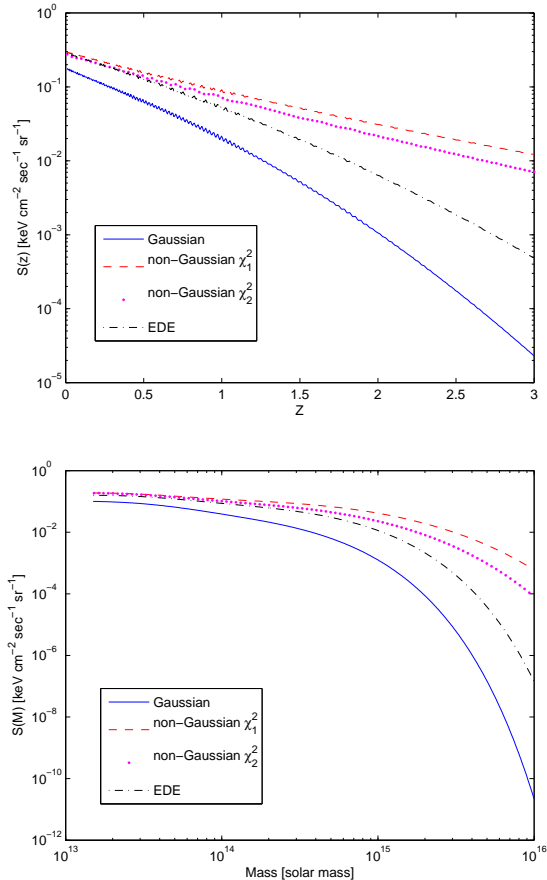


Figure 10. The redshift (top panel) and mass (bottom panel) distributions of the CXRB spectral intensity contributed by clusters are shown for the Gaussian (blue solid curve), χ_1^2 (red dashed curve), χ_2^2 (purple dotted curve) PDFs, and for the EDE model (black dot-dashed curve).

to the corresponding value in Λ CDM leads to similar predicted spectra. This conclusion is valid even if we adopt $C_{gas} = 5$, in addition to using the WMAP5-deduced σ_8 , which is higher by $\sim 10\%$ than the corresponding WMAP3 value (adopted here). The impact of the higher value of σ_8 is illustrated in Fig. 6.

4 DISCUSSION

Significant advancements in sensitivity and spatial resolution have resulted in an improved ability to resolve the XRB into its different components and sources. The combination of high quality data and enhanced-accuracy calculations can be used in order to constrain different aspects which affect directly and indirectly the XRB levels. As elaborated upon in § 3.1, the spectral bump in the band $0.4 \lesssim E \lesssim 1$ keV, an important characteristic of line emission from high-mass groups and poor clusters, constitutes a particularly sensitive probe; models which boost the emission in this energy band might exceed the XRB data. Another important observational constraint includes the XRB levels in the hard energy band, $2-10$ keV. It seems to have been established that AGN constitute the major contributors in this energy

band. Consequently, models in which the cluster contribution is appreciably higher than $\sim 10\% - 20\%$ of the total CXRB intensity would likely be non-viable. Moreover, the combination of extensive measurements of the CXRB and detailed predictions of the contributions of AGN, clusters, and starburst galaxies, provide a diagnostic tool of the number density and evolution of these sources, as well as a probe to set constraints on alternative cosmological models.

We demonstrated in this paper that meaningful constraints can be set on alternative cosmological models by contrasting the predicted contribution of clusters to the CXRB in non-Gaussian χ_m^2 and EDE models with the measurements. As discussed in § 1, there seems to be some observational evidence for earlier cluster formation and higher abundances (as compared with those in Λ CDM) that are predicted in these models. Our basic result is that the cluster contribution in the χ_1^2 and χ_2^2 models is excessively high at low ($\lesssim 1$ keV) energies, so much so that these models could probably be ruled out. Moreover, in the high energy band, 2 – 10 keV, the predicted spectral intensity attains unrealistically high levels by virtue of the fact that most of the CXRB at these energies originates in AGN. The viability of the EDE model considered here depends very much on how exactly this model is normalized with respect to the standard model. With the same σ_8 as derived from WMAP5 values, the predicted energy bump in this EDE model exceeds the measured range, as is the case in the non-Gaussian models. However, normalizing σ_8 such that the cumulative halo number at $z = 0$ in this model matches the corresponding value in Λ CDM, yields nearly the same spectrum. These conclusions are still valid even if we adopt $C_{gas} = 5$ and Galactic absorption with $b_{min} = 10^\circ$, along with ST mass function and the value of σ_8 deduced from WMAP5 measurements, which is higher by $\sim 10\%$ than the corresponding WMAP3 value. The effect of this increment in σ_8 is illustrated in Fig. 6.

We also showed how the CXRB can be used to constrain merger scenarios. We estimated the impact of mergers heuristically by determining the resulting boost in the CXRB in terms of the change in σ_8 and Ω_m , following the work of RSR02. CXRB levels calculated for two of the three models exceed the observational data in the spectral bump region. The 20% increment of σ_8 leads to an overproduction of the XRB intensity levels, also when adopting $C_{gas} = 5$ and the WMAP5 parameters, whereas a 10% boost is in marginal agreement with the data (for a more detailed account of the models see § 6). The impact of Galactic absorption, neglected in these calculations, is discussed in § 3.2.

We explored the impact of non-gravitational heating on the CXRB and found only a minor change. While the spectral bump is not affected at all, higher energy emission from clusters decreases in proportion with the amount of non-gravitational heating. Nonetheless, this decrement is small, unless non-gravitational heating is considerable. Changing the polytropic index, γ , from 1 (isothermal) to 1.25 also does not alter the spectrum considerably, especially for low C_{gas} . With $C_{gas} = 10$ and $\gamma = 1.25$ the central temperature is higher and the temperature at large radii, $r \gtrsim r_{vir}$ is lower than with the $\gamma = 1$ case. However, since the integration of the mass and gas profiles is performed up to the virial radius, we only notice an enhancement of the spectrum levels

at high energies. For $C_{gas} = 5$ there is almost no difference between the $\gamma = 1$ and $\gamma = 1.25$ cases.

It was shown that inclusion of all relevant emission processes (i.e., not just Bremsstrahlung) is very important. Especially important is line emission, which generates the $0.4 \lesssim E \lesssim 1$ keV spectral bump. We calculated the spectrum taking mean abundances of 0 and 0.3 solar. In clusters the metallicity is typically ~ 0.2 solar outside the central region (Baldi et al. 2007; Leccardi & Molendi 2008). The Fe abundance is nearly similar in all hot clusters, > 4.5 keV (Mushotzky 2004 and reference within), even though medium temperature clusters, 2–4 keV, have abundances of ~ 0.4 (Baumgartner et al. 2005). There seems to be a slight redshift dependence; XMM and Chandra show no evolution in Fe abundances up to $z \approx 0.8$ (e.g., Mushotzky 2004 and reference within). However, a certain degree of enrichment must have occurred. Balestra et al. (2007) found that the average iron content of IC gas at $z = 0$ is a factor ~ 2 higher than at $z \approx 1.2$. Several low-redshift, bright X-ray groups were shown by Finoguenov & Ponman (1999) to have Fe abundances of $\lesssim 0.3$ at radii higher than ~ 100 kpc. For almost any kind of abundance gradient and evolution the CXRB contributions of high mass groups and clusters is between our derived values for $A = 0$ and $A = 0.3$.

The impact of using a mass function different than PS was explored by repeating the calculations with the ST mass function, which is characterised by higher abundances of high-mass halos in the mass range $M > 4 \cdot 10^{13} h_{0.7}^{-1} M_\odot$ with respect to the corresponding numbers predicted by the PS mass function. The enhanced abundances result in appreciably higher intensity levels that possibly exceed the measured XRB range for high values of C_{gas} even in Λ CDM. Clearly, given that not all of the XRB in the $0.4 \lesssim E \lesssim 1$ keV energy range is due to high-mass groups and clusters, this implied excess provides a very tight constraint on the maximum value of C_{gas} . (Note that the mass range of the Jenkins et al. (2001) mass function, which was deduced from N-body simulations, is irrelevant to our work here.) If $C_{gas} \approx C_{DM}$, where C_{DM} is the concentration parameter, the XRB can put strong constraints on the value of the concentration parameter.

Finally, we note that whereas we have accounted for emission from groups and clusters, our treatment does not include emission from the filamentary WHIM. With temperatures $\sim 10^6$ or slightly higher, WHIM emission could also contribute somewhat to the CXRB. Clearly, any additional contribution will only strengthen our conclusions on the viability of alternative models in which the predicted spectral bump exceeds the observed range.

ACKNOWLEDGMENT

We wish to thank the anonymous referee for a thorough reading of a previous version of the paper and for several useful suggestions.

REFERENCES

- Baldi, A., Etori, S., Mazzotta, P., Tozzi, P., & Borgani, S. 2007, *ApJ*, 666, 835
- Balestra, I., Tozzi, P., Etori, S., Rosati, P., Borgani, S., Mainieri, V., Norman, C., & Viola, M. 2007, *A&A*, 462, 429
- Bardeen, J. M., Bond, J. R., Kaiser, N., & Szalay, A. S. 1986, *ApJ*, 304, 15
- Bartelmann, M., Doran, M., & Wetterich, C. 2006, *A&A*, 454, 27
- Bauer, F. E., Alexander, D. M., Brandt, W. N., Schneider, D. P., Treister, E., Hornschemeier, A. E., & Garmire, G. P. 2004, *Astron. J.*, 128, 2048
- Baumgartner, W. H., Loewenstein, M., Horner, D. J., & Mushotzky, R. F. 2005, *ApJ*, 620, 680
- Binney, J., & Tremaine, S. 1987, Princeton, NJ, Princeton University Press, 1987, 747 p.,
- Brandt, W. N., & Hasinger, G. 2005, , 43, 827
- Broadhurst, T. J., & Barkana, R. 2008, *MNRAS*, 390, 1647
- Broadhurst, T., Umetsu, K., Medezinski, E., Oguri, M., & Rephaeli, Y. 2008, *Ap. J. Lett.*, 685, L9
- Bullock, J. S., Kolatt, T. S., Sigad, Y., Somerville, R. S., Kravtsov, A. V., Klypin, A. A., Primack, J. R., & Dekel, A. 2001, *MNRAS*, 321, 559
- Caldwell, R. R., Doran, M., Müller, C. M., Schäfer, G., & Wetterich, C. 2003, *Ap. J. Lett.*, 591, L75
- Cowie, L. L., Garmire, G. P., Bautz, M. W., Barger, A. J., Brandt, W. N., & Hornschemeier, A. E. 2002, *Ap. J. Lett.*, 566, L5
- Dawson, K. S., Holzapfel, W. L., Carlstrom, J. E., Joy, M., & LaRoque, S. J. 2006, *ApJ*, 647, 13
- De Luca, A., & Molendi, S. 2004, *A&A*, 419, 837
- Dickey, J. M., & Lockman, F. J. 1990, , 28, 215
- Doran, M., Schwindt, J.-M., & Wetterich, C. 2001, *Phys. Rev. D.*, 64, 123520
- Finoguenov, A., & Ponman, T. J. 1999, *MNRAS*, 305, 325
- Gendreau, K. C., et al. 1995, *Publ. Astron. Soc. Japan*, 47, L5
- Georgantopoulos, I., Stewart, G. C., Shanks, T., Boyle, B. J., & Griffiths, R. E. 1996, *MNRAS*, 280, 276
- Giacconi, R., Gursky, H., Paolini, F. R., & Rossi B. B., 1962, *Phys. Rev. Lett.*, 9, 439
- Giacconi, R., et al. 2001, *ApJ*, 551, 624
- Gilli, R., Risaliti, G., & Salvati, M. 1999, *A&A*, 347, 424
- Gilli, R., et al. 2003, *ApJ*, 592, 721
- Gilli, R., Comastri, A., & Hasinger, G. 2007, *A&A*, 463, 79
- Gruber, D. E. 1992, *The X-ray Background*, 44
- Gruber, D. E., Matteson, J. L., Peterson, L. E., & Jung, G. V. 1999, *ApJ*, 520, 124
- Hasinger, G., Burg, R., Giacconi, R., Schmidt, M., Trumper, J., & Zamorani, G. 1998, *A&A*, 329, 482
- Hasinger, G. 2004, *Nuclear Physics B Proceedings Supplements*, 132, 86
- Hickox, R. C., & Markevitch, M. 2006, *ApJ*, 645, 95
- Hickox, R. C., & Markevitch, M. 2007, *Ap. J. Lett.*, 661, L117
- Itoh, N., Sakamoto, T., Kusano, S., Nozawa, S., & Kohyama, Y. 2000, *Ap. J. Supp.*, 128, 125
- Jenkins, A., Frenk, C. S., White, S. D. M., Colberg, J. M., Cole, S., Evrard, A. E., Couchman, H. M. P., & Yoshida, N. 2001, *MNRAS*, 321, 372
- Komatsu, E., et al. 2009, *Ap. J. Supp.*, 180, 330
- Koyama, K., Soda, J., & Taruya, A. 1999, *MNRAS*, 310, 1111
- Kuo, C. L., et al. 2004, *ApJ*, 600, 32
- Kurk, J., Venemans, B., Röttgering, H., Miley, G., & Pentericci, L. 2004, *Astrophysics and Space Science Library*, 301, 141
- Kushino, A., Ishisaki, Y., Morita, U., Yamasaki, N. Y., Ishida, M., Ohashi, T., & Ueda, Y. 2002, *Publ. Astron. Soc. Japan*, 54, 327
- Leccardi, A., & Molendi, S. 2008, *A&A*, 487, 461
- Lemze, D., Barkana, R., Broadhurst, T. J., & Rephaeli, Y. 2008, *MNRAS*, 386, 1092 (L08a)
- Lemze, D., Broadhurst, T., Rephaeli, Y., Barkana, R., & Umetsu, K. 2008, arXiv:0810.3129 (L08b)
- Lockman, F. J., Jahoda, K., & McCammon, D. 1986, *ApJ*, 302, 432
- Loken, C., Norman, M. L., Nelson, E., Burns, J., Bryan, G. L., & Motl, P. 2002, *ApJ*, 579, 571
- Lumb, D. H., Warwick, R. S., Page, M., & De Luca, A. 2002, *A&A*, 389, 93
- Maggiore, M., & Riotto, A. 2009, arXiv:0903.1250
- Magliocchetti, M., Silva, L., Lapi, A., de Zotti, G., Granato, G. L., Fadda, D., & Danese, L. 2007, *MNRAS*, 375, 1121
- Markevitch, M., Forman, W. R., Sarazin, C. L., & Vikhlinin, A. 1998, *ApJ*, 503, 77
- Mathis, H., Diego, J. M., & Silk, J. 2004, *MNRAS*, 353, 681
- Miley, G. K., et al. 2004, *Nature*, 427, 47
- Mushotzky, R. F., Cowie, L. L., Barger, A. J., & Arnaud, K. A. 2000, *Nature*, 404, 459
- Mushotzky, R. 2004, *Frontiers of X-ray astronomy*, 149
- Navarro, J. F., Frenk, C. S., & White, S. D. M. 1997, *ApJ*, 490, 493 (NFW)
- Peebles, P. J. E. 1971, *A&A*, 11, 377
- Phillips, L. A., Ostriker, J. P., & Cen, R. 2001, *Ap. J. Lett.*, 554, L9
- Ponman, T. J., Bourner, P. D. J., Ebeling, H., Bohringer, H. 1996, *MNRAS*, 283, 690
- Press, W. H., & Schechter, P. 1974, *ApJ*, 187, 425
- Randall, S. W., Sarazin, C. L., & Ricker, P. M. 2002, *ApJ*, 577, 579 (RSR02)
- Readhead, A. C. S., et al. 2004, *ApJ*, 609, 498
- Revnivtsev, M., Gilfanov, M., Sunyaev, R., Jahoda, K., & Markwardt, C. 2003, *A&A*, 411, 329
- Rosati, P., della Ceca, R., Norman, C., & Giacconi, R. 1998, *Ap. J. Lett.*, 492, L21
- Sadeh, S., Rephaeli, Y., & Silk, J. 2006, *MNRAS*, 368, 1583
- Sadeh, S., Rephaeli, Y., & Silk, J. 2007, *MNRAS*, 380, 637
- Sadeh, S., & Rephaeli, Y. 2008, *MNRAS*, 388, 1759
- Sheth, R. K., & Tormen, G. 1999, *MNRAS*, 308, 119
- Sheth, R. K., Mo, H. J., & Tormen, G. 2001, *MNRAS*, 323, 1
- Spergel, D. N., et al. 2007, *Ap. J. Supp.*, 170, 377
- Tozzi, P., & Norman, C. 2001, *ApJ*, 546, 63
- Vecchi, A., Molendi, S., Guainazzi, M., Fiore, F., & Parmar, A. N. 1999, *A&A*, 349, L73
- Voit, G. M., Kay, S. T., & Bryan, G. L. 2005, *MNRAS*, 364, 909

- Warwick, R. S., & Roberts, T. P. 1998, *Astronomische Nachrichten*, 319, 59
- Wetterich, C. 2004, *Physics Letters B*, 594, 17
- Worsley, M. A., et al. 2005, *MNRAS* , 357, 1281
- Worsley, M. A., Fabian, A. C., Bauer, F. E., Alexander, D. M., Brandt, W. N., & Lehmer, B. D. 2006, *MNRAS* , 368, 1735
- Wu, X.-P., & Xue, Y.-J. 2001, *ApJ* , 560, 544
- Yang, Y., Mushotzky, R. F., Barger, A. J., Cowie, L. L., Sanders, D. B., & Steffen, A. T. 2003, *Ap. J. Lett.* , 585, L85